



**Inducing nano-confined crystallization in semicrystalline polymers by elastic melt stretching**

Journal:	<i>Soft Matter</i>
Manuscript ID	SM-COM-12-2020-002181.R2
Article Type:	Communication
Date Submitted by the Author:	18-Jan-2021
Complete List of Authors:	Razavi, Masoud; University of Akron College of Polymer Science and Polymer Engineering, Zhang, Wenwen; University of Science and Technology of China, National Synchrotron Radiation Lab Hefei, CN, Khonakdar, Hossein Ali; Iran Polymer and Petrochemical Institute, Janke, Andreas; 2Leibniz-Institute of Polymer Research Dresden, Dept. of Nanostructured Materials Li, Liangbin; University of Science and Technology of China, National Synchrotron Radiation Lab Wang, Shi-Qing; University of Akron, Polymer Science

## **Inducing nano-confined crystallization in semicrystalline polymers by elastic melt stretching**

Masoud Razavi<sup>1</sup>, Wenwen Zhang<sup>2</sup>, Hossein Ali Khonakdar<sup>3,4</sup>, Andreas Janke<sup>3</sup>, Liangbin Li<sup>2\*</sup>  
and Shi-Qing Wang<sup>1\*</sup>

<sup>1</sup>College of Polymer Science and Engineering, University of Akron, Akron, OH44325

<sup>2</sup>National Radiation Laboratory, University of Science and Technology of China, Hefei, China

<sup>3</sup>Leibniz Institute of Polymer Research, D-01067 Dresden, Germany

<sup>4</sup>Iran Polymer and Petrochemical Institute, P.O. Box 14965/115, Tehran, Iran

### **Abstract**

Based on two widely studied semicrystalline polymers, poly (L-lactic acid) (PLLA) and polyethylene terephthalate (PET) of high glass transition temperature  $T_g$ , this Letter shows that these brittle materials can be made to be super tough, heat resistant and optically clear by creating nano-sized crystals while preserving the entanglement network. Atomic force microscopic images confirm the perceived nano-crystallization. Time-resolved X-ray scattering/diffraction measurements reveal the emergence of cold crystallization during either stress relaxation from large stepwise melt-stretching of PLLA and PET or annealing of pre-melt-stretched PLLA and PET above  $T_g$ . Mechanical tests show that the polymers in this new state are extraordinarily tough and strong even well above  $T_g$ , e.g., above 100 °C.

---

\* Corresponding authors: [lbl@ucst.edu.cn](mailto:lbl@ucst.edu.cn), [swang@uakron.edu](mailto:swang@uakron.edu)

One frontier in polymer physics is the subject of molecular mechanics of semicrystalline polymers (SCPs). Unlike other modern materials, polymeric materials are uniquely ductile. While SCPs have earned a considerable reputation as modern materials with high specific mechanical strength, a great deal of improvement could still be expected upon further chain-level understanding of the physics governing the ductility of SCPs. It is well known that upon increasing either the degree of crystallinity<sup>1</sup> or the average size of spherulites<sup>2</sup> even polyethylene (PE) and polypropylene (PP) can lose drawability. Moreover, we find that glassy SCPs are typically brittle. For example, PP turns brittle below its  $T_g$ .<sup>3,4</sup> Such adverse effects of crystallization on toughness has made it hard for the promising bio-based poly(L-lactic acid) (PLLA) to replace the petroleum-based polyethylene terephthalate (PET).

In our judgment, when a SCP crystallizes to form space-filling spherulites, the chain network can be disrupted relative to its structure in the molten state. Specifically, lamellar crystallization depletes the interchain uncrossability constraints since strands pack in parallel in lamellae. For a SCP to be ductile is for its crystalline phase to yield, i.e., to undergo plastic transformation. Spherulites in SCPs must undergo shape changes during ductile uniaxial drawing. In general shape changes of spherulites involve breakdown of the lamellae. Therefore there is no guarantee that such crystal melting<sup>5</sup> or fragmentation<sup>6,7</sup> can occur without failure of the underlying chain network. This is especially true when a SCP is drawn below its glass transition temperature  $T_g$ .

A great deal of recent efforts have focused on how external deformation near and above melt crystallization temperature  $T_c$  induces crystallization, e.g., creating shish-kebab like crystalline morphology<sup>8-13</sup> or nano-oriented crystals,<sup>14</sup> most often involving isotactic PP (iPP). While predeformation of molten iPP, as involved in the making of iPP fibers, has been explored<sup>15</sup> to make it ductile in the glassy state, little is understood about why drawing iPP in its crystalline state can achieve comparable improvement. Our recent unpublished study confirms that a much stronger iPP can be produced with predrawing in the crystalline state.

In this work, we describe a different approach and perspective, aiming to identify an effective way to enhance mechanical and thermal performance for a family of SCPs, which we term type B. Type B SCPs are defined as semicrystalline polymers with higher  $T_g$  than room temperature and slow crystallization kinetics so that they can be fast thermally quenched from their molten states into a glassy state without crystallization. PET and PLLA belong to this class. Having type B SCPs in their amorphous state provides us an opportunity to explore the possibility of having crystallization without disrupting the chain network.

In passing, it is worth mentioning that strain-induced crystallization of type B SCPs has been investigated for a long time. For example PET can be made to crystallize faster continuous hot-drawing.<sup>16-20</sup> There are also attempts to model the deformation behavior during SIC processes.<sup>21, 22</sup> When hot drawing is done in the affine deformation limit so that the geometric condensation effect<sup>23</sup> can result, crystalline PET can be expected to have enhanced strength when examined in the hot drawing direction, according to our recent revelation of the crucial role of chain networking.<sup>24, 25</sup> Indeed, a more recent study showed enhanced mechanical properties after elongational crystallization.<sup>26</sup>

Thus, we envision the following scenario to achieve considerable crystallization while preserving the integrity of the chain network. Let us consider bringing an amorphous SCP above its  $T_g$  to temperature  $T_{ms}$ . We choose  $T_{ms}$  that the SCP at  $T_{ms}$  ( $> T_g$ ) does not undergo cold crystallization over a specific period of time  $t_{exp}$  due to lack of sufficient molecular mobility. This experimental time window is long enough for us to subject the SCP to either uniaxial or biaxial extension. Here and hereafter, we refer to this procedure as melt stretching. It is well known<sup>27</sup> that polymers of high molecular weight above  $T_g$  can be elastically stretched to a substantial stretching ratio  $\lambda_{ms}$ , e.g., 3, without encountering significant chain disentanglement that would lead to structural failures of various kinds.<sup>28,29</sup> We can apply a sufficiently high extensional Hencky rate  $\dot{\epsilon}$  relative to the Rouse relaxation time  $\tau_R(T_{ms})$  i.e., the Rouse-Weissenberg number  $Wi_R = \dot{\epsilon}\tau_R > 1$ , so that the entanglement network is substantially melt-stretched to a stretching ratio  $\lambda_{ms}$  in the elastic limit tensile strain localization. Here the degree of chain orientation depends on  $Wi_R$  and  $\lambda_{ms}$ . If sufficient molecular orientation is produced by the melt stretching, it is plausible that in presence of the significant chain alignment cold crystallization would immediately take place on the length scale of the network mesh size.

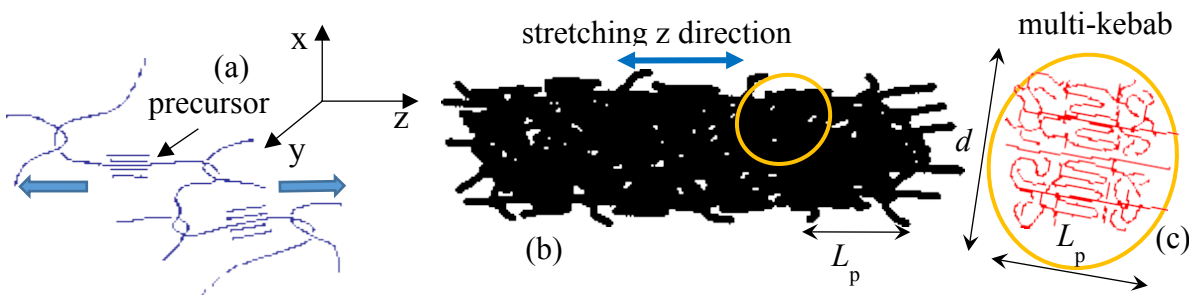


Fig. 1 (a) Elastic stretching of a chain network to create precursors, i.e., highly aligned entanglement strands for cold crystallization at temperature  $T_{ms}$  ( $> T_g$ ) where cold crystallization would not occur in absence of the melt stretching. (b) Upon full crystallization, a web of connected kebab confined within the network mesh size, leaving the network intact. The stretched meshes define the cylinder-shaped clusters with diameter  $d$  and height  $L_p$ . (c) The characteristic dimension of the confined domains,  $L_p$ , is defined by the size of the stretched mesh whereas the lateral dimension  $d$  depends the regularity of the chain network.

Specifically, as shown Fig. 1(a), we foresee a rapid emergence of precursors for nano-confined crystallization (NCC) associated with the highly stretched strands in the entanglement network. The crystal sizes can be expected to be nanoscopic for several reasons. First, the density of nucleation sites should be as high as defined by the mesh size, which can be taken as the entanglement spacing for simplicity. Second, upon crystallization that acts like crosslinking, the chain network locks up so that no disentanglement due to the high chain retraction force could take place. Consequently, no strands can escape from the interchain uncrossability constraint, thus limiting the available strands per nucleation site for crystallization. More explicitly, as sketched in Fig. 1(b), it is reasonable to propose a specific morphology, involving a network of connected

small lamellae, where each lamella may be in the shape of short cylinders of diameter  $d$  and height  $L_p$  (including an interlamellar amorphous layer), as shown in Fig. 1(c).

In this Letter, based on PLLA and PET, we set out to present a successful demonstration of NCC as envisioned from the preceding theoretical considerations. Two protocols are available to achieve such scale-controlled, network-preserved cold crystallization. In both scenarios, a type B SCP in its amorphous state is brought above its  $T_g$  at  $T_{ms}$  and subjected to melt stretching. Beyond a threshold of stretching ratio  $\lambda^*$ , cold-crystallization appears to take place, judging from the stress vs. strain curve, as described in the Supporting Information. In the first protocol, the melt stretching is terminated before reaching  $\lambda^*$  to commence the stress relaxation in anticipation that cold crystallization could be induced by the melt stretching. As shown in Fig. 2(a), the tensile stress is found to decline until it turns negative as the crystallizing specimen increases its length because of the directional crystallization. Such a new PLLA is optically transparent (as shown in the inset of Fig. 6), suggesting that the crystal sizes are well below the wavelength of visible light. To confirm crystallization, *ex situ* wide-angle-X-ray diffraction (WAXD) measurements are carried out to show in the inset of Fig. 2(a) that there is indeed oriented crystallization.

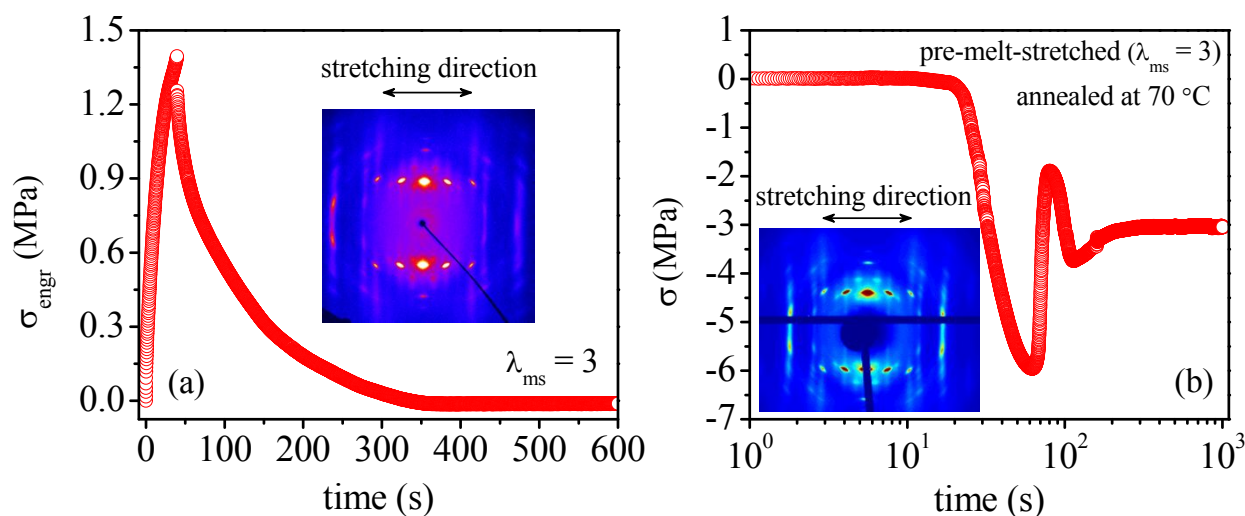


Fig. 2 (a) Stress growth upon stepwise melt stretching of PLLA at  $T = 70$  °C, ten degrees above  $T_g$  at Hencky rate  $\dot{\epsilon} = 0.027$  s $^{-1}$  and stress relaxation at  $\lambda_{ms} = 3$ . The inset photo is *ex situ* WAXD characterization at the end of the stress relaxation. (b) Stress reading upon annealing at 70 °C of a PLLA that has been melt-stretched to  $\lambda_{ms} = 3$  and immediately quenched. The inset photo is *ex situ* WAXD characterization of the sample at the end of the annealing.

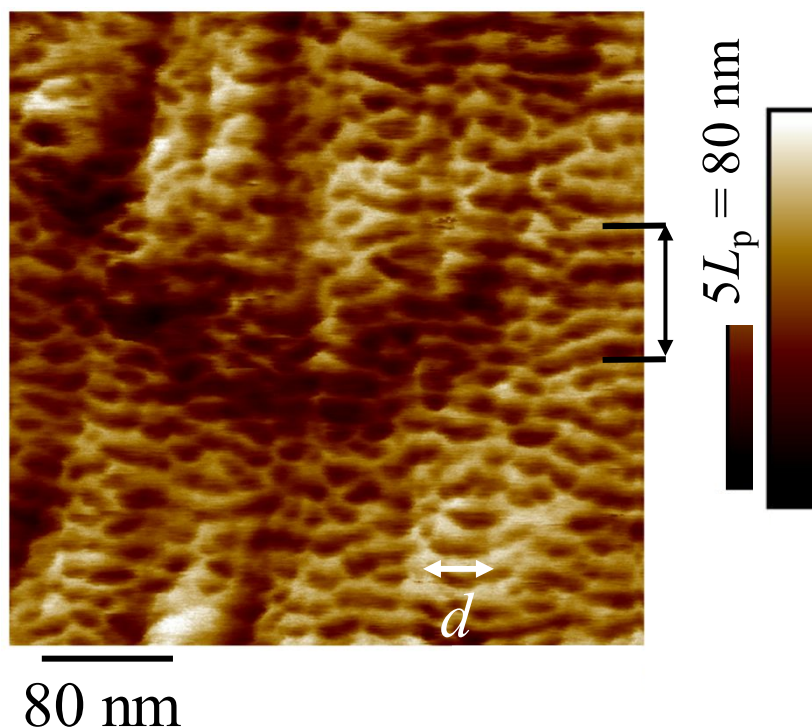


Fig. 3 AFM image of the annealed pre-melt-stretched PLLA, revealing a unique morphology of the crystalline phase, consisting a family of "cylinders", separated by the lighter (softer) regions. The image was taken at 80 °C, showing the Derjaguin-Muller-Toporov modulus in an arbitrary unit (a.u.) – see Supporting Information. The cylinders are vertically (along the direction of stretching) separated by an average distance  $L_p = \text{ca. } 15 \text{ nm}$ , with an average height shorter than 15 nm and diameter  $d$  varying from one to a few of  $L_p$ .

Based on type B SCPs as PLLA and PET, it is straightforward to carry out melt-stretching at  $T_{\text{ms}} (> T_g)$  to a stretching ratio of  $\lambda_{\text{ms}}$  and preserve the resulting chain orientation by rapid thermal quenching to room temperature. The pre-melt-stretched PLLA and PET remain amorphous in storage at room temperature. When it is heated to a temperature  $T_2 > T_g$ , cold crystallization may be induced by holding such specimens fixed between two clamps of an Instron tester. For the detailed description of this second protocol, see Supporting Information. The second protocol affords us the additional control over the condition for the stretch-induced NCC since  $T_2$  can be chosen to be different from  $T_{\text{ms}}$ . Here  $T_2$  is below the quiescent crystallization temperature  $T_{\text{cc}}$ , where an undeformed amorphous polymer attains maximum cold crystallization kinetics, which is 102 °C for PLLA and 166 °C for PET according to our DSC measurements presented in Supporting Information. We choose  $T_2 = 70 \text{ °C}$  for PLLA, just 10 degrees above  $T_g$ . Fig. 2(b) shows the annealing process in terms of the measured stress: The pre-melt stretched PLLA starts to heat up at  $t = 20 \text{ s}$ , and the thermal expansion causes the specimen to bend to generate negative stress. As the temperature rises above  $T_g$  at  $t = 60 \text{ s}$ , the specimen begins to contract, correspondingly the stress starts to be less negative. The emergence of NCC prevents elastic yielding<sup>30</sup> so that the

specimen remains bent. The explanation is confirmed by the *ex situ* WAXD pattern given in the inset of Fig. 2(b). The *ex situ* WAXD pattern in the inset of Fig. 2(b) indeed confirms that the new transparent PLLA crystalline.

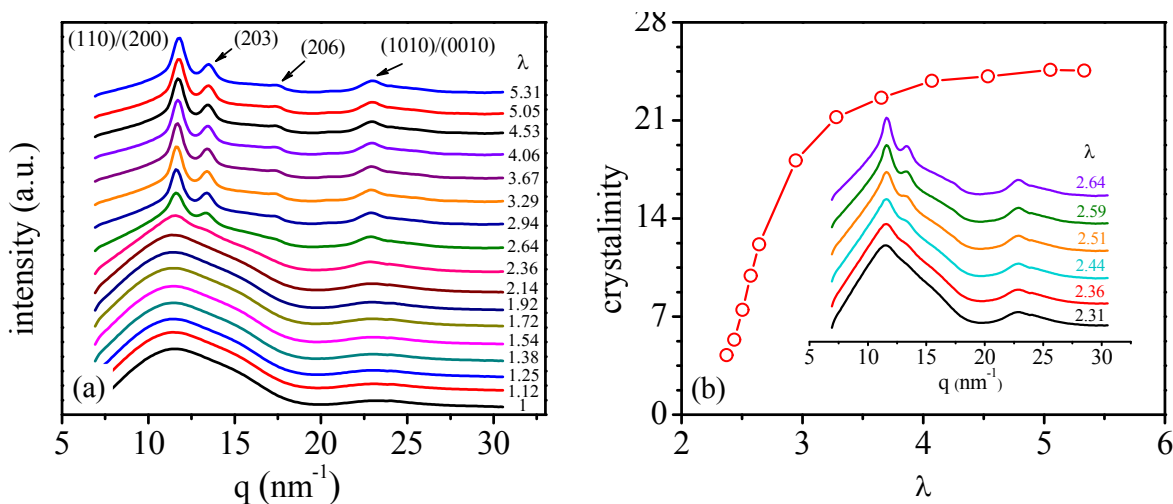


Fig. 4 (a) Time-resolved WAXD measurements during uniaxial melt stretching of PLLA at 70 °C and Hencky rate  $\dot{\epsilon} = 0.027 \text{ s}^{-1}$  up to  $\lambda = 5.5$ , revealing a series of characteristic structural information. (b) Degree of crystallinity as a function of the stretching ratio  $\lambda$ . The inset shows the abrupt emergence of crystallization over a narrow range of  $\lambda$ .

To gain insights into the molecular mechanism for NCC, depicted in Fig. 1(a)-(b), atomic force microscopic (AFM) measurements were carried out on a ncc-PLLA obtained using the second protocol, i.e., annealing of pre-melt-stretched PLLA as described in Fig. 2(b). Here ncc-PLLA stands for nano-confined crystallized PLLA. The AFM image in Fig. 3 of ncc-PLLA and shows a spatial feature that could be identified with nano-sized crystals depicted in Fig. 1(b)-(c), with  $L_p = 15 \text{ nm}$  and  $d$  varying from one to three in the unit of  $L_p$ .

To firmly establish such an approach to create NCC in certain SCPs, we perform *in situ* X-ray scattering in both wide-angle (WAXD) and small-angle (SAXS) modes. At 70 °C, according to the differential scanning calorimetry, the well-aged PLLA in its amorphous state would not undergo any discernible crystallization in half an hour. However, crystallization can be induced during melt stretching according to Fig. S.1 in Supporting Information. Time-resolved WAXD measurements are carried out to show in Fig. 4(a)-(b) that considerable crystallization indeed starts to emerge around  $\lambda = 2.5$ , which is also signified by the rise of the tensile stress in Fig. S.1. The degree of crystallinity grows sharply from  $\lambda = 2.5$  to  $\lambda = 3.5$ , reaching 25% during the melt stretching at Hencky rate  $= 0.027 \text{ s}^{-1}$ , as indicated in Fig. 4(b).

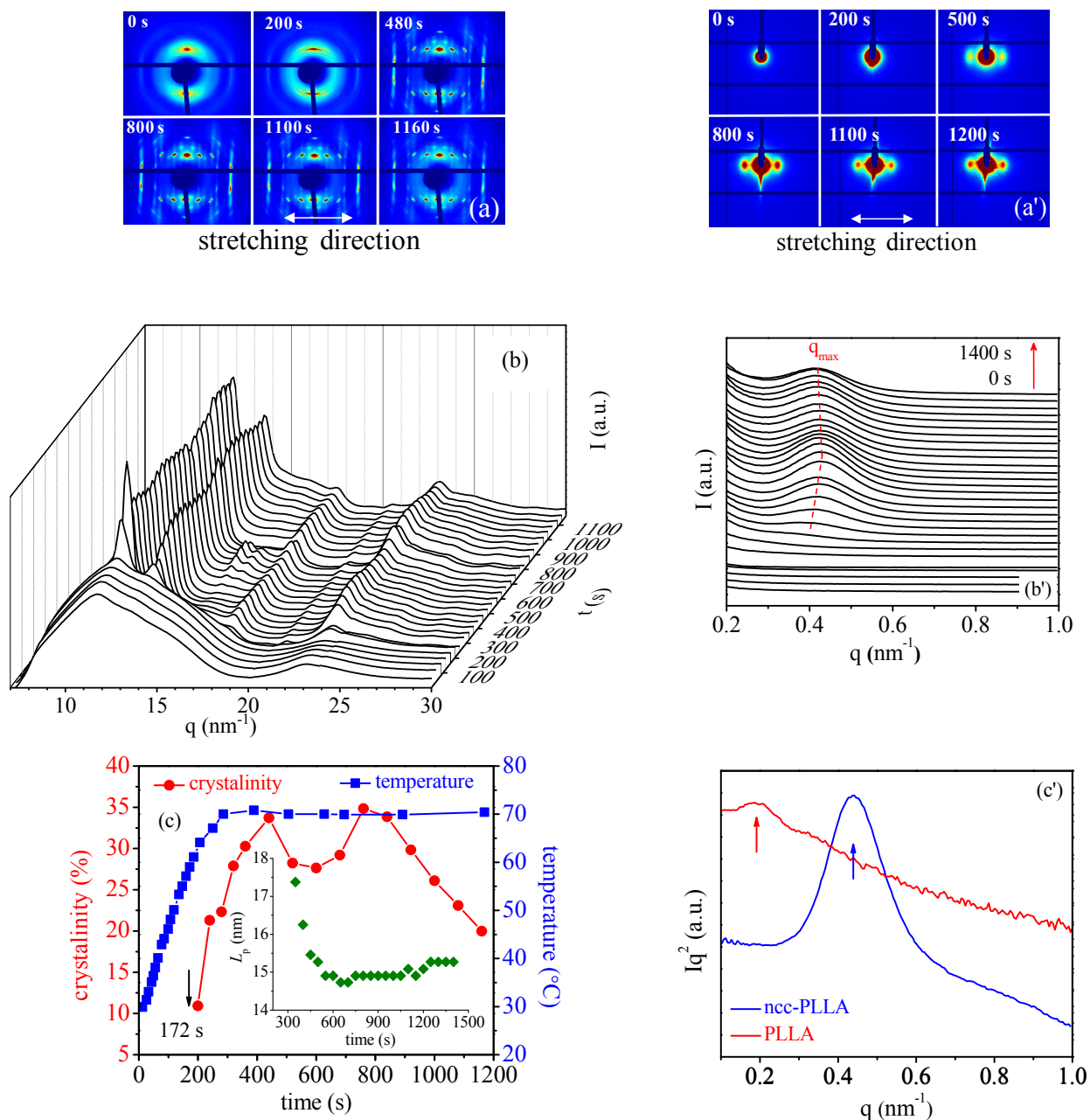


Fig. 5 Time-resolved 2D patterns of (a) WAXD and (a') SAXS at different times during annealing at 70 °C of a pre-melt-stretched PLLA, which results in ncc-PLLA. Temporal evolutions of (b) WAXD intensity profiles along the equatorial direction and (b') SAXS intensity profiles along the meridional direction. (c) Emergent crystallinity (left Y axis), evaluated from data in (b), and temperature profile (right Y axis) as a function of time, with the inset showing the SAXS measurement of the long period  $L_p$ , obtained from (b'). (c') Calibrated SAXS intensities in terms of  $Iq^2$  (Lorentz correction)<sup>31</sup> to reveal a change in the long period  $L_p = 2\pi/q_{\max}$  from 30 nm for the quiescently crystallized PLLA, to 15 nm in ncc-PLLA.



Time-resolved WAXD and SAXS capability also permits us to detect the formation of the cold crystallization during annealing of pre-melt-stretched PLLA and PET. Specifically, during the annealing, which is described in Fig. 2(b) for PLLA, both WAXD and SAXS measurements are carried out as a function of time. Fig. 5(a) and (a') show the respective WAXD and SAXS patterns at the various times. Fig. 5(b) and (b') present the characteristic  $q$  dependence of the scattering intensities at both wide and small angles as a function of time. As indicated in Fig. 5(c), the NCC becomes discernible as the pre-melt-stretched PLLA heats up across  $T_g = 60$  °C at 172 s. The crystallinity shoots up to ca. 35%, as shown by the circles in Fig. 5(c), followed by a drop and rise before a further decrease of the crystallinity beyond  $t = 800$  s. Clearly, the crystallization and melting have alternated, where the melting is plausibly driven by the persistent chain tension produced by the pre-melt-stretching. Tracing the peak positions of the SAXS intensity in Fig. 5(b'), we can also determine the long period  $L_p = 2\pi/q_{\max}$  as a function of the annealing time and find in the inset of Fig. 5(c) that  $L_p$  locks onto a value around 15 nm. It is important to note that this value quantitatively agrees with the average separation of the cylindrical crystals along the stretching direction, as shown in Fig. 3.

It is interesting to discuss the meaning of  $L_p$  revealed by the SAXS measurements in the context of Fig. 1(b) and Fig. 3. According to our sketch, the average inter-crystal separation should have a distance no smaller than  $\lambda_{\text{ms}}$  times the mesh size of the entanglement network. If the mesh size can be taken as the equilibrium entanglement spacing<sup>32</sup>  $l_{\text{ent}0} = \text{ca. } 4.4$  nm,  $L_p$  should be at least 13.2 nm. According to the AFM and SAXS measurements,  $L_p = 15$  nm in support of the basic idea (cf. Fig. 1) that has guided us to create the new NCC. The AFM image also shows  $d > L_p$ , implying that the lamellae are not restricted by the lateral mesh size. If it is restricted to the mesh width of  $l_{\text{ent}0}/(\lambda_{\text{ms}})^{1/2} \sim 2.5$  nm, we would have observed  $d \sim 2.5$  nm, instead of values greater than  $L_p = 15$  nm. The lateral lamellar growth is limited by the irregularities of the chain network. Therefore, the lateral dimensions are also bounded. According to Fig. 3, the lamellae could be cylindrical with a diameter  $d$ , typically no greater than three times  $L_p$ , i.e.,  $d$  varying from  $L_p$  to  $3L_p$ .

For SCPs that have higher  $T_g$  than room temperature and slow crystallization kinetics, we can bypass crystallization and prepare them in their amorphous form in order to achieve NCC. Such crystallization preserves the structural integrity of the geometrically-condensed<sup>24</sup> chain network and therefore could make glassy SCPs super tough and strong. As an illustration of the remarkable mechanical improvement, Fig. 6 compares the stress vs. strain curves of one ordinary PLLA, cold crystallized in absence of any predeformation and the other being ncc-PLLA. The contrast is sharp: PLLA is brittle at room temperature (RT) and hardly drawable above  $T_g$ , and the ncc-PLLA is superbly tough at room temperature and remarkably strong even above  $T_g$ . Finally, it is worth mentioning that the transparent ncc-PLLA shows outstanding thermal stability, e.g., able to retain its dimension at 120 °C (well above  $T_g$ ) for over 30 min, suggesting that the nano-sized crystals are space filling and jammed up, as sketched in Fig. 1(b). We have verified that the same protocols that permit the creation of ncc-PLLA described in Fig. 2 through Fig. 5 apply to PET. See Supporting Information for the results on PET. The present protocol might prove effective in practice when combined with the compounding approach to hasten crystallization in PLLA and PET as demonstrated by Tonelli.<sup>33, 34</sup> Unlike the modified PLLA and PET<sup>34</sup> that are

expected to have folded-chain crystals, the crystalline morphology of our ncc-PLLA and ncc-PET, as revealed in the AFM image in Fig.3, is most plausibly non-spherulitic, involving extended-chain crystallites confined to the mesh size of the entanglement network.

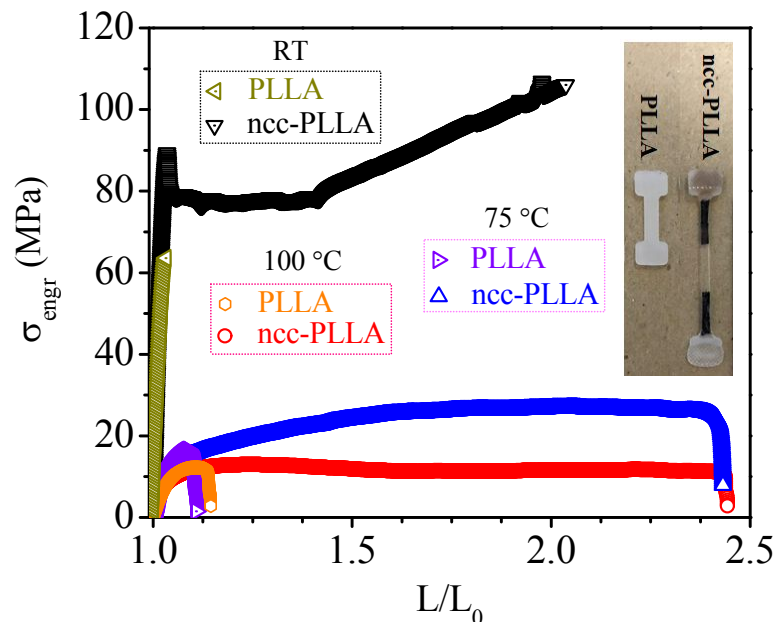


Fig. 6 Engineering stress vs. draw ratio during uniaxial extension along the same direction as melt stretching with  $V/L_0 = 0.5 \text{ min}^{-1}$ , at room temperature as well as 75 and 100 °C, for the ncc-PLLA produced using the method described in Fig. 2(a) as well as the untreated PLLA.  $L_0 = 30$  and 35 mm respectively for PLLA and ncc-PLLA specimens. The inset image compares the appearance of milky PLLA and transparent ncc-PLLA.

In summary, we have identified effective ways to produce a new crystalline state through cold crystallization of melt-stretched PLLA and PET where only nano-sized crystals exist. The new morphology is a connected web of nanoscopic crystals, grouped into clusters of cylindrical shape with various diameters. The new crystalline phase, made of these clusters, is space filling, pushing heat distortion temperature to melting temperature of PLLA near 160 °C. The ncc-PLLA and ncc-PET are superbly ductile and optically transparent, presenting itself as a promising next-generation polymeric materials.

This work is supported, in part, by a grant (DMR-1905870) from the Polymers program of the National Science Foundation. Zhang and Li acknowledge support from the National Natural Science Foundation of China (51633009).

## References

1. L. Mandelkern, F. L. Smith, M. Failla, M. A. Kennedy and A. J. Peacock, *J. Polym. Sci. Pt. B-Polym. Phys.*, 1993, **31**, 491-493.
2. G. Ehrenstein and R. P. Theriault, *Applications. Hanser. Cincinnati*, 2001.
3. A. Van der Wal, J. Mulder, H. Thijs and R. Gaymans, *Polymer*, 1998, **39**, 5467-5475.
4. A. van der Wal, J. J. Mulder and R. J. Gaymans, *Polymer*, 1998, **39**, 5477-5481.
5. P. J. Flory, *Nature*, 1978, **272**, 226-229.
6. A. Peterlin, *Journal of materials science*, 1971, **6**, 490-508.
7. A. Peterlin, *Colloid and polymer science*, 1987, **265**, 357-382.
8. G. Kumaraswamy, R. K. Verma, J. A. Kornfield, F. Yeh and B. S. Hsiao, *Macromolecules*, 2004, **37**, 9005-9017.
9. R. H. Somani, L. Yang, L. Zhu and B. S. Hsiao, *Polymer*, 2005, **46**, 8587-8623.
10. A. Elmoumni and H. H. Winter, *Rheologica acta*, 2006, **45**, 793-801.
11. F. G. Hamad, R. H. Colby and S. T. Milner, *Macromolecules*, 2015, **48**, 3725-3738.
12. B. Nazari, H. Tran, B. Beauregard, M. Flynn-Hepford, D. Harrell, S. T. Milner and R. H. Colby, *Macromolecules*, 2018, **51**, 4750-4761.
13. K. Cui, Z. Ma, N. Tian, F. Su, D. Liu and L. Li, *Chemical reviews*, 2018, **118**, 1840-1886.
14. K. N. Okada, J.-i. Washiyama, K. Watanabe, S. Sasaki, H. Masunaga and M. Hikosaka, *Polym. J.*, 2010, **42**, 464-473.
15. Y. Zhu, N. Okui, T. Tanaka, S. Umemoto and T. Sakai, *Polymer*, 1991, **32**, 2588-2593.
16. X. Lu and J. Hay, *Polymer*, 2001, **42**, 8055-8067.
17. D. Salem, *Polymer*, 1992, **33**, 3189-3192.
18. F. Rietsch, *European polymer journal*, 1990, **26**, 1077-1080.
19. A. Thompson, *Journal of polymer science*, 1959, **34**, 741-760.
20. E. Dargent, A. Denis, C. Galland and J. Grenet, *Journal of thermal analysis*, 1996, **46**, 377-385.
21. S. Ahzi, A. Makradi, R. Gregory and D. Edie, *Mechanics of materials*, 2003, **35**, 1139-1148.
22. C. Buckley, D. Jones and D. Jones, *Polymer*, 1996, **37**, 2403-2414.
23. G. D. Zartman, S. Cheng, X. Li, F. Lin, M. L. Becker and S.-Q. Wang, *Macromolecules*, 2012, **45**, 6719-6732.
24. S.-Q. Wang, S. Cheng, P. Lin and X. Li, *The Journal of chemical physics*, 2014, **141**, 094905.
25. M. Razavi, S. Cheng, D. Huang, S. Zhang and S.-Q. Wang, *Polymer*, 2020, 122445.
26. K. Okada, Y. Tanaka, H. Masunaga and M. Hikosaka, *Polym. J.*, 2018, **50**, 167-176.
27. S.-Q. Wang, *Nonlinear Polymer Rheology: Macroscopic phenomenology and Molecular foundation*, Wiley, Hoboken, NJ, 2018.
28. A. Y. Malkin and C. J. S. Petrie, *J. Rheol.*, 1997, **41**, 1-25.
29. X. Zhu and S.-Q. Wang, *J. Rheol.*, 2012, **57**, 223-248.
30. Y. Wang, P. Boukany, S.-Q. Wang and X. Wang, *Phys. Rev. Lett.*, 2007, **99**, 237801.
31. B. B. He, *Two-dimensional X-ray diffraction*, Wiley Online Library, 2009.
32. M. Razavi and S.-Q. Wang, *Macromolecules*, 2019, **52**, 5429-5441.
33. A. S. Joojode, K. Hawkins and A. E. Tonelli, *Macromolecular Materials and Engineering*, 2013, **298**, 1190-1200.
34. A. E. Tonelli, *Polymer Crystallization*, 2020, **3**, e10095.